ESTUDIO QUÍMICO DEL CÚMULO GLOBULAR NGC-5927

(CHEMICAL STUDY OF THE GLOBULAR CLUSTER NGC-5927)

TESIS PARA OPTAR AL GRADO ACADÉMICO DE

MAGÍSTER EN CIENCIAS CON MENCIÓN EN FÍSICA

POR

ALDO ANDRÉS MURA GUZMÁN

Profesor Guía: Dr. Sandro Villanova
Departamento de F'isica
Facultad de Ciencias Físicas y Matemáticas
Universidad de Concepción

Comisión: Dr. Sandro Villanova
Dr. Douglas Geisler
Dr. Dominik Schleicher

Abril, 2017

Concepción, Chile

Acknowledgements

Abstract

Globular Clusters (GCs) are natural laboratories where stellar and chemical evolution can be studied in detail. In addition, their chemical patterns and kinematics can tell us which Galactic structure (Disk, Bulge, Halo or extragalactic) the cluster belongs to. NGC 5927 is one of most metal-rich GCs in the Galaxy and its kinematics links it to the Thick Disk. We present abundance analysis based on high resolution spectra of 7 giant stars. The data were obtained using FLAMES/UVES spectrograph mounted on UT2 telescope of the Very Large Telescope (VLT) of the European Southern Observatory. The principal motivation of this work is to perform a wide and detailed chemical abundance analysis of the cluster and look for possible Multiple Populations (MPs). We determined stellar parameters and measured 22 elements corresponding to light (Na, Al), alpha (O, Mg, Si, Ca, Ti), iron-peak (Sc, V, Cr, Mn, Fe, Co, Ni, Cu, Zn) and heavy elements (Y, Zr, Ba, Ce, Nd, Eu). We found a mean iron content of [Fe/H]=-0.47 $\pm$0.02. We confirm the existence of MPs in this GC with an O-Na anti-correlation, and moderate spread in Al abundances. We estimate a mean [α/Fe]=0.25 $\pm$0.08. Iron-peak elements shows no significant spread. The [Ba/Eu] ratios indicate a predominant contribution from SNeII for the formation of the cluster.

Contents

List of Figures

List of Tables

Chapter 1

Introduction

Galactic Globular Clusters (GGCs) are considered as natural laboratories for the study of different stellar evolution processes, and they are among the oldest objects in the universe. We can compare GCs with the different components of the Milky Way looking for inter-relationships in their chemistry and/or kinematics. The Galaxy is made-up by at least 3 main structures: The Halo, the Bulge and the Disk. This last one is suggested to have two major distinct sub-components: Thick Disk and Thin Disk (Gilmore & Reid, 1983) where GGCs can be found in each one of these structures. (See Figure 1.1 as an example). The differences between the Galaxy components is exhibited in the metallicity, abundance enhancements, age and kinematics among others which can be observed in GGC too.
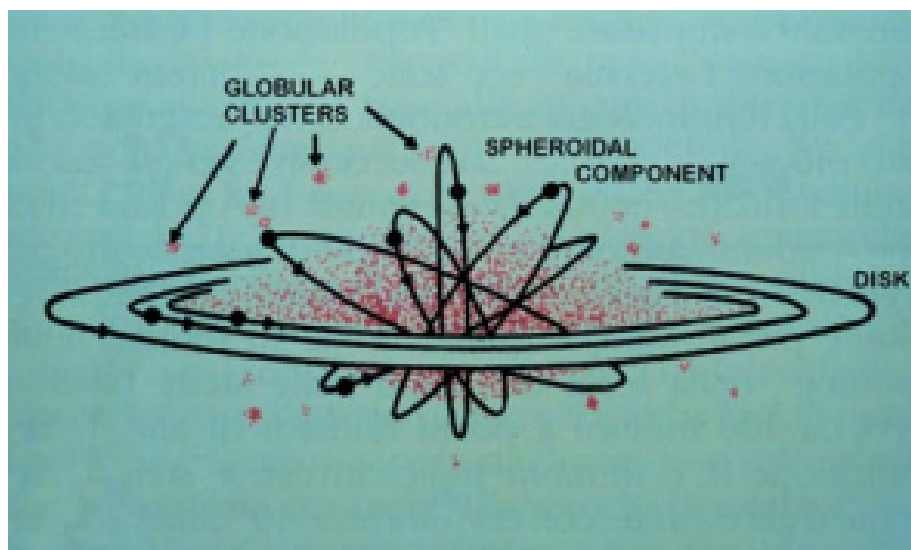
Figura 1.1: Representation of the distribution of GCs in the Milky Way (Murdin, 2001).

When we talk about the Galactic Bulge, we are reffering to an important structure of the Milky Way which mass estimations goes from the 10% (Oort, 1977) to the 25% Sofue et al. (2009) of the total stellar mass in the Milky Way. Ortolani et al. (1995) and Zoccali et al. (2003) have estimated an age about $t = 10 \pm 2.5$ Gyr for the bulk of the metal-rich population of the Galactic Bulge and its kinematics behaviour is dominated by a rotationally supported system with a rotational peak of $\sim$75 km s^{-1} (Minniti, 1996; Beaulieu et al., 2000; Rich et al., 2007), in addition to a high velocity dispersion (Minniti, 1996) which decreases along the distance from the Galactic center.

Meanwhile, the Thin and Thick Disk structures have different stellar populations observed for the first time by Gilmore & Reid (1983) studying the stellar density at difference Galactic latitudes towards the Galactic North pole. Much observational evidence (Gratton et al., 2000; Mashonkina & Gehren, 2001; Reddy et al., 2003, 2006; Adibekyan et al., 2012) indicates that both sub-structures have different chemical origins and have passed through different chemical evolution. The stellar population of the Thick Disk host old stars within 8 to 10 Gyr while the Thin disk stars shows younger ages (Bensby et al., 2003; Schuster et al., 2006).

A completely different structure is the Halo which is constituted by stars and GCs spherically distributed surrounding the Bulge and Disk. The Halo is much less massive than the Bulge or Disk with an estimated stellar mass of $M_s = 4 - 7 \times 10^8$ M$_\odot$, about 1% of the Galaxy's stellar mass (Bland-Hawthorn & Gerhard, 2016). In addition, the stars hosted in the Halo are generally old and metal-poor.

Not long ago, stars in GCs were originally considered coeval (Renzini & Buzzoni, 1986) and initially chemically homogeneous. Today, we know that GCs host Multiple Populations (MPs) in their stellar content and both photometric and spectroscopic methods are used in order to understand this phenomenon. Using spectroscopy we can observe spreads in the light element contents (C, N, O, Na, Mg, Al) forming patterns between them as correlations or anti-correlations. These signatures come from different reactions (Denisenkov & Denisenkova, 1989; Langer et al., 1993) which are simultaneously active, depleting some light elements and enhancing others. These reactions are carried out by proton capture during Hydrogen burning at high temperature ($\sim 15 \times 10^6$K for CNO chain, $\sim 30 \times 10^6$K for NeNa chain and $\sim 70 \times 10^6$K for MgAl chain) achieved in relatively massive stars (M $\geqslant$ 2M$_\odot$). Figure 1.2 shows the diagram for the three cycles.
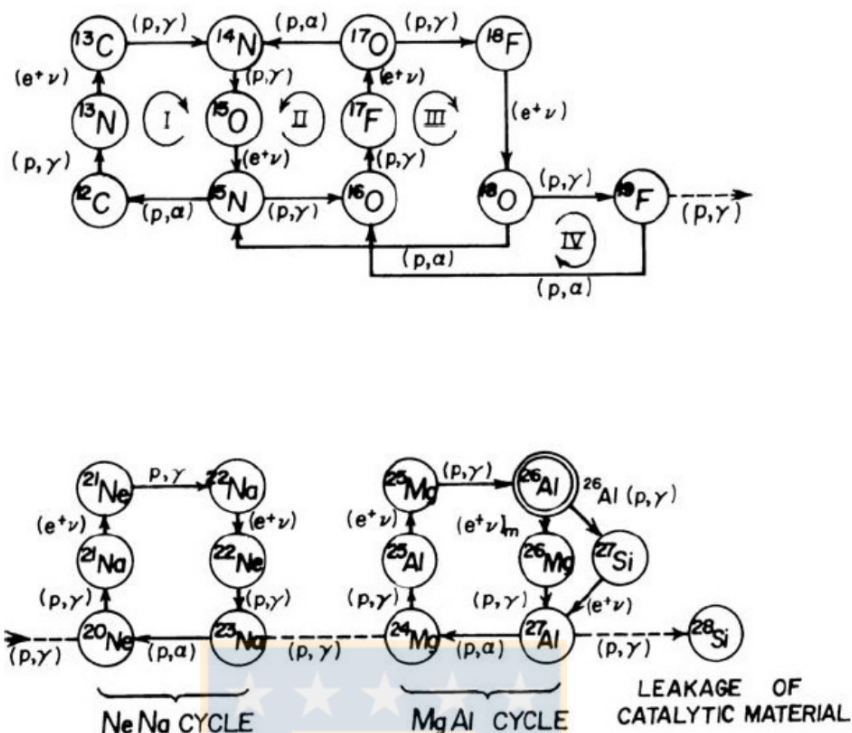
Figura 1.2: Diagrams for the CNO, Ne-Na and Mg-Al cycles (Pagel, 1997).

The feature best studied is the Na-O anti-correlation (Carretta et al., 2009a,b). Every GGC (and others extra-Galactic GCs) we know so far follows this pattern with the only exception of Ruprecht 106, which possible extragalactic origin (Villanova et al., 2013) might be an explanation for its observed SSP. Figure 1.3 shows the O-Na anti-correlation in 19 GGCs where the shape and extension of the feature varies from cluster-to-cluster, but it is present in all the sample. This anti-correlation between Na and O is probably due to the evolution of massive stars in early stages of the GC. A First Generation (FG) of stars (i.e. Na-rich O-poorer) polluted the intra-cluster gas left behind with processed material and then a second generation (SG) of stars was formed being Na-richer and O-poorer (Caloi & D'Antona, 2011). There are several candidates for this light element polluter: intermediate mass AGB stars (D'Antona et al., 2002), fast rotating massive MS stars (Decressin et al., 2007) and massive binaries (de Mink et al., 2009). However, none of the proposed scenarios to date is able to account for all of the observed MP phenomena and a new theory is badly needed.

On the other hand, heavy elements are produced by neutron capture. This process can be slow (s-process) or rapid (r-process), depending on the ratio of the time scales of neutron capture to beta decay. These processes are carried out in AGB stars for the s-process or SNeII explosions for the

r.process and their relative abundances give us an idea about which process contributed more in the chemical evolution of the cluster as we will discuss later.
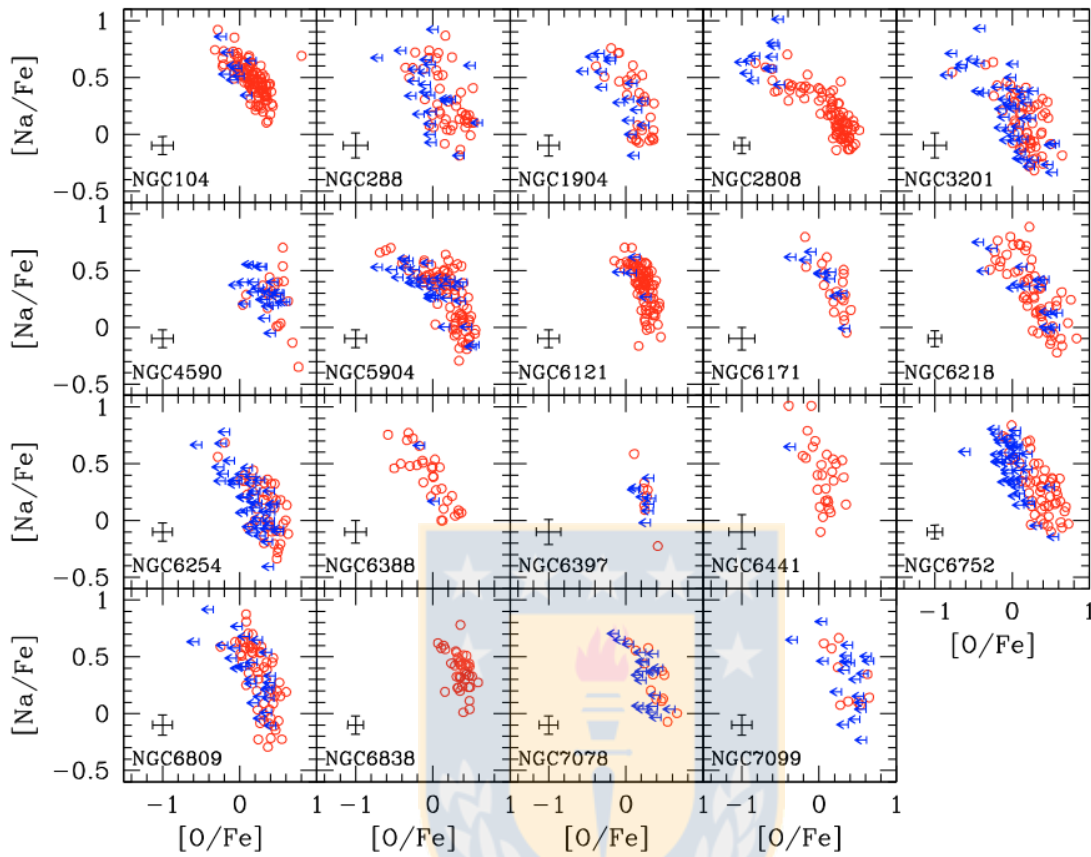
Figura 1.3: Carretta et al. (2009a) : Na-O anti-correlation in 19 GGCs

The estimation of chemical abundances can be made by photometric or spectroscopic analysis. From the photometry some estimations can be done. If an element is more abundant, the absorption line will be deeper, implying a lower intensity in a certain wavelength range which can be studied with a filter sensitive to these variations. The differences in chemical abundances from star-to-star in a cluster can give us information, for example, about its MPs.

Chemical abundances derived from spectroscopy give us accurate values where two techniques are the most used and powerful: equivalent widths (EWs) and spectrum-synthesis. Both methods require an atmospheric model and a line list with the spectral lines information as input in order for the program to identify . The EWs correspond to a geometrical method where the area of the absorption line is identical to a rectangle considered under the normalized continuum in a intensity flux-wavelength diagram, where the base of the rectangle is at 0 flux and whose width yields the same area as measured in the actual line. The width of the rectangle is given by the following

definition for the EW's equation:

$$W_\lambda = \int_{\lambda_1}^{\lambda_2} (1 - F_\lambda/F_0)d\lambda,$$

where F_λ is the intensity across the the wavelength range between λ_1 and λ_2, F_0 correspond to the continuum intensity which is generally normalized. A representation of both, the observed spectral line and the rectangle constructed is shown in figure 1.4 as an example.
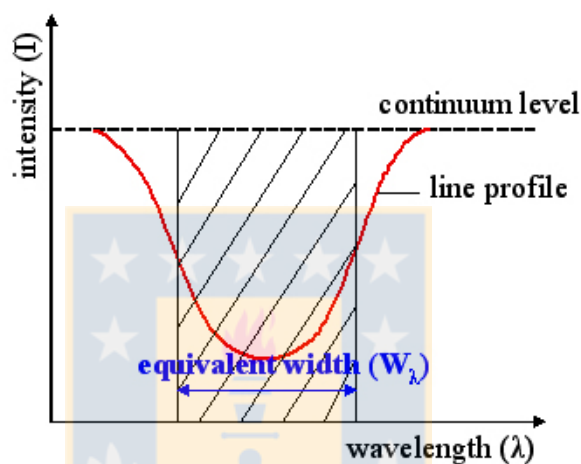
Figura 1.4: Representation of EWs method for chemical abundances estimations (Image created by Dorottya Szam).

The other analysis method is the spectrum-synthesis which basically compares the observed spectrum with a synthetic one. This method has the advantage to compare spectral lines which are not so deep and can not be measured via EWs, mainly because of their strong blending with other lines. During the fitting process the synthetic spectrum can be modify by setting the continuum, the full width half maximum (FWHM) and the abundance of the measured element, among others parameters, in order to recreate as best as possible the spectral line. At the end of the fitting process, the chemical abundance can be estimated with with high accuracy. An example of this method is represented in figure 3.1.

In this work we present a chemical study of the GC NGC 5927 based on high resolution spectra taken from UVES. This cluster is very old with an age of 12.25 Gyr (Dotter et al., 2010) which means that it was formed during the earliest stages of the Galaxy formation and could give us a hint

about how the initial material got processed chemically. About kinematics, Casetti-Dinescu et al. (2007) and Allen et al. (2008) concluded that the orbital parameters of NGC 5927 is consistent with that of a rotationally supported system, suggesting this GC belongs to the Thick Disk. In terms of chemical abundances instead, there is a lack of studies using high resolution spectra. Many attempts have been made in order to estimate its metallicity based on low- resolution Ca_{II} IR triplet measurements (Rutledge et al., 1997) before 2013. Then, in the catalogue performed by Harris (1996, ed. 2010), a value of [Fe/H]=-0.49 dex was obtained by averaging metalicities derived from Armandroff & Zinn (1988), Francois (1991) and Carretta et al. (2009c). Finally, the most recent study about chemical analysis related to NGC 5927 was performed by Pancino & the GES collaboration (2017, Hereafter P17) where their study was focused in the Mg-Al anti-correlation in 9 GCs including NGC 5927. The elements presented in P17 are Fe, O, Na, Mg and Al which we are going to compare with our measurements. In addition, P17 and us are the first high-resolution studies of NGC 5927, which is the optimum method to derive detailed abundances for a large number of species with a variety of nucleosynthetic origins.

In Section 2 we describe the observations and data reduction performed for the study. Section 3 is a description of the methods used in order to derive the chemical abundances and the errors analysis. In Section 4 our results are presented and compared with different components of the Galaxy and other GCs and finally in Section 5 we give a summary, present our findings and proffer our conclusions.

Chapter 2

Observations and Data Reduction

The dataset consist of high resolution (R $\sim$ 40000) spectra of 7 giant stars from NGC 5927 using the Ultraviolet Echelle Spectrograph (UVES) (Dekker et al., 2000) on the VLT .The central wavelength was centered in 580 nm and the spectral range covers between 480 nm and 620 nm (CCD#3, filter SHP700, red arm only). Each star spectrum is the combination of spectra from 20 observing block (OB) with an exposure time of 3600 s for each OB. The data was obtained from the ESO Archive[1] as public data. The selection of targets was made using a CMD based on observations with the Advanced Camera for Surveys (ACS) on-board Hubble Space Telescope and the spatial distribution of the observed stars is shown in figure 2.1 including the core radius and the half mass-radius. Allen et al. (2008) calculated a tidal radius for NGC 5927 using **?** formula (R_K) and a reduced King's formula (R_*) in two different potential. In an axisymmetric potential R_K=52.1pc and R_*=61.5pc but under a barred potential R_K=49.8pc and R_*=57.6pc. For a more detailed explanation about the target selection and data reduction, please see Simmerer et al. (2013, Sections 3 and 4). Regarding to the star sample, there seems to be two AGB stars in our data which we marked with a circle in case of strange behaviours.

---

[1]Observations were made in ESO facilities on VLT-UT2 telescope, Cerro Paranal, under program ID 079.B-0721(A).
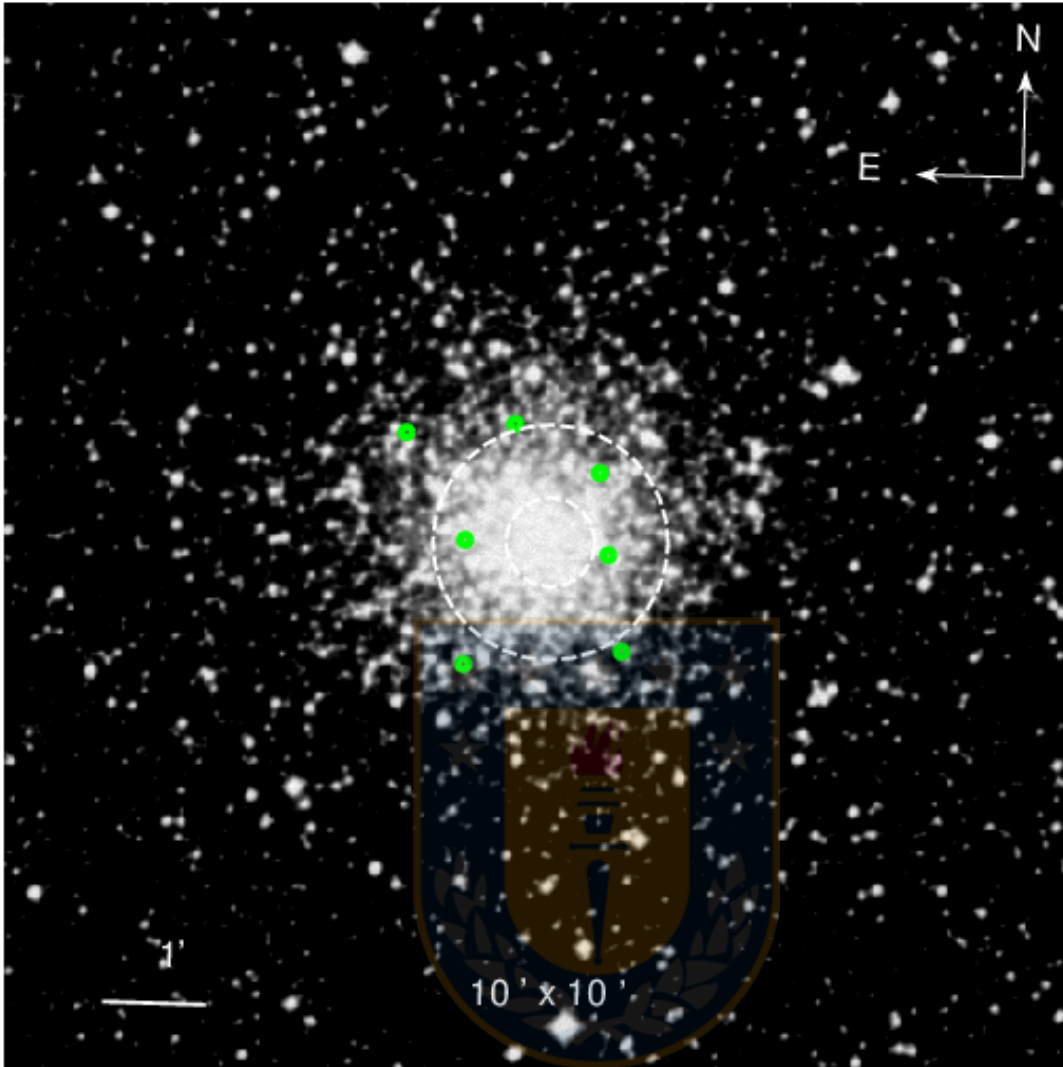
Figura 2.1: A 10' × 10' digitized sky survey image centered on NGC 5927. North is up and east to the left. The green symbols show the location of the spatial distribution of the 7 stars analyzed. The dashed circles correspond to the core radius, r_c=0.42', and half mass-radius, r_h=1.10' (Harris 1996, 2010 ed).

Star	604.7-605.3 nm	606.8-607.6 nm
1	48.13	50.24
2	41.36	35.05
3	39.72	37.54
4	30.58	36.00
5	34.82	40.56
6	36.95	40.30
7	47.64	49.49

Tabla 2.1: Estimation of the signal-to-noise ratio in each star between 604.7-605.3 nm and 606.8-607.6 nm.

The signal-to-noise ratio (S/N) in our spectra is between 20-50 at ~ 600 nm. Table 2.1 shows the S/N of each star in two different wavelength ranges. About data reduction, bias subtraction, flat-field correction and wavelength calibration were performed using the UVES pipeline version 5.7.0[2]. The sky subtraction, and spectral rectification were performance using *Sarith* and *continuum* tasks in IRAF.

Radial velocities were measured using the *fxcor* task in IRAF and a synthetic spectrum as a template. Radial velocities indicate that the 7 stars are members of the cluster and we found a mean radial velocity of $v_r = -102.45 \pm 3.50$ km s^{-1}. This value is in good agreement with Simmerer et al. (2013), who found a mean radial velocity of $v_r = -104.03 \pm 5.03$ km s^{-1} for the cluster using the same UVES data, but also GIRAFFE data (72 member stars).

The position of NHC 5927 in the Galaxy is shown in Figure 2.2 with a distance about 4.6 kpc from de Galactic center and a height compatible with the Thick Disk. Also, its Galactic coordinates are *l*=326.60, *b*=4.86 (degrees).

---

[2]Pipelines list on http://www.eso.org/sci/software/pipelines/.
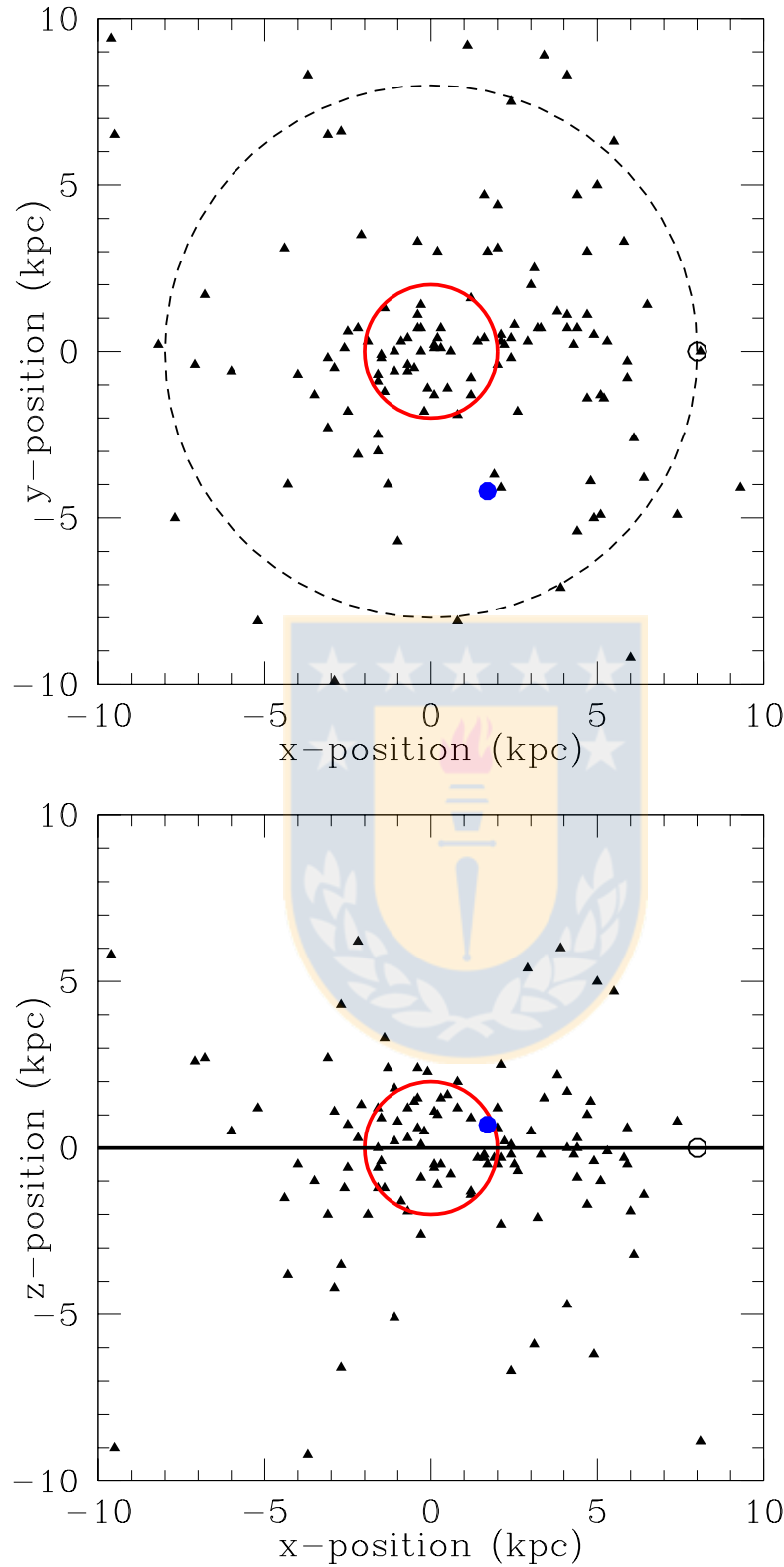
Figura 2.2: Position of NGC 5927 with respect to the Galactic Center. Filled blue circle represent NGC 5927 and filled black triangles GCs from Harris (1996, 2010 ed.). Dashed line is the distance from the Galactic Center to the Sun $R_{\odot}$=8 kpc, red circle is the Bulge radius with R_{bulge}=2 kpc and the black line is the Galactic plane. *Upper panel*: Represent X-Y plane and *Lower panel*: X-Z plane

Chapter 3

Abundance Analysis.

Because NGC 5927 is close to the Galactic plane as show in Figure 2.2 ($b = 4.86°$), its extinction is relatively significant. Heitsch & Richtler (1999) found a total reddening of $E_{V-I} = 0.43 \pm 0.02$ and a maximum differential reddening of $\Delta E_{V-I}^{MAX} = 0.27$. In order to avoid errors introduced by photometric estimations due to the strong extinction, we derive stellar parameters using spectra.

We used the Local Thermodynamic Equilibrium (LTE) MOOG program (Sneden, 1973) for the abundance analysis coupled with ATLAS9 (Kurucz, 1970) atmospheric models. For the analysis we used spectral linelists from Villanova & Geisler (2011) and the solar abundances listed in column 10 of Table 3.2.

Tabla 3.1: Basic parameters of our star sample in NGC 5927.

ID	RA$_{fibre}$ (deg)	DEC$_{fibre}$ (deg)	V$_{F606W}$ (mag)	I$_{F814W}$ (mag)	RV_H (km/s)	T_{eff} (K)	$\log(g)$ (dex)	v_t (km/s)	[Fe/H]
1	232.02279	-50.67275	16.04	15.82	-105.279	4519	2.61	1.10	-0.54
2	231.99008	-50.66175	16.16	15.98	-101.163	4500	2.60	1.21	-0.49
3	232.02242	-50.69211	16.19	16.09	-102.328	4835	2.86	1.59	-0.44
4	232.01121	-50.65447	16.03	15.88	-105.656	4422	2.56	1.40	-0.47
5	231.98354	-50.68953	16.02	15.83	-102.252	4430	2.52	1.22	-0.51
6	232.03792	-50.65622	16.08	15.88	-105.538	4376	2.28	1.06	-0.37
7	231.98742	-50.67450	16.12	15.94	-94.948	4358	2.24	0.96	-0.49

The atmospheric parameters were obtained varying the effective temperature (T_{eff}), microturbulent velocity (v_t) and gravity ($log(g)$) in order to remove any trend between the excitation potential and equivalent width vs. abundance, and to satisfy the ionization equilibrium respectively. The FeI and FeII were used for this latter purpose. The [Fe/H]value of the model was changed at each iteration according to the output of the abundance analysis. The final derived

stellar parameters for each star used in the analysis are listed in Table 3.1.

Two different techniques were used to obtain the element abundances from our spectra. The Ca, Ti V, Cr, Fe, Co and Ni abundances were measured using Equivalent Widths ((Marino et al., 2008, see EWs)). For O, Na, Mg, Al, Si, Sc, Mn, Cu, Zn, Y. Zr, Ba, Ce, Nd and Eu we used the spectrum-synthesis method because of the blending with other spectral lines. For each line we calculated 5 synthetic spectra varying the abundance. The value that minimizes the rms fit to the observations is our final estimation. Figure 3.1 is an example of the fitting process in Mn and Al absorption lines in Star #2. We selected lines not contaminated by telluric lines and we made special considerations for Ba and Na. We took hyperfine splitting into account for the Ba measurements and the Na abundances were corrected for non-LTE (NLTE) using corrections provided by the INSPEC [1] database.

In addition, a detailed internal error analysis was performed by varying T_{eff}, $\log(g)$, [Fe/H], and v_t by an amount equal to the estimated internal error in each parameter. Then Abundances in star #2 was re-measure, assuming that it represent the entire sample. The parameters were varied by $\Delta T_{eff} = +65$ K, $v_t = +0.08$ Km s^{-1}, $\Delta \log(g) = +0.09$ and $\Delta[Fe/H] = +0.03$ dex. This estimation of the internal errors for atmospheric parameters was performed as in Marino et al. (2008). The results of errors are listed in Table 3.3, including errors due to the noise in the spectra. This error was obtained for elements whose abundance was obtained by EQWs, as the average value of the errors of the mean given by MOOG, and for elements whose abundance was obtained by spectrum-synthesis, as the error given by the fitting procedure. The σ_{tot} is the square-root of the sum of the squares of the individual errors, while σ_{obs} is the mean observed dispersion for each element.

---

[1] http://inspect.coolstars19.com/index.php?n=Main.HomePage
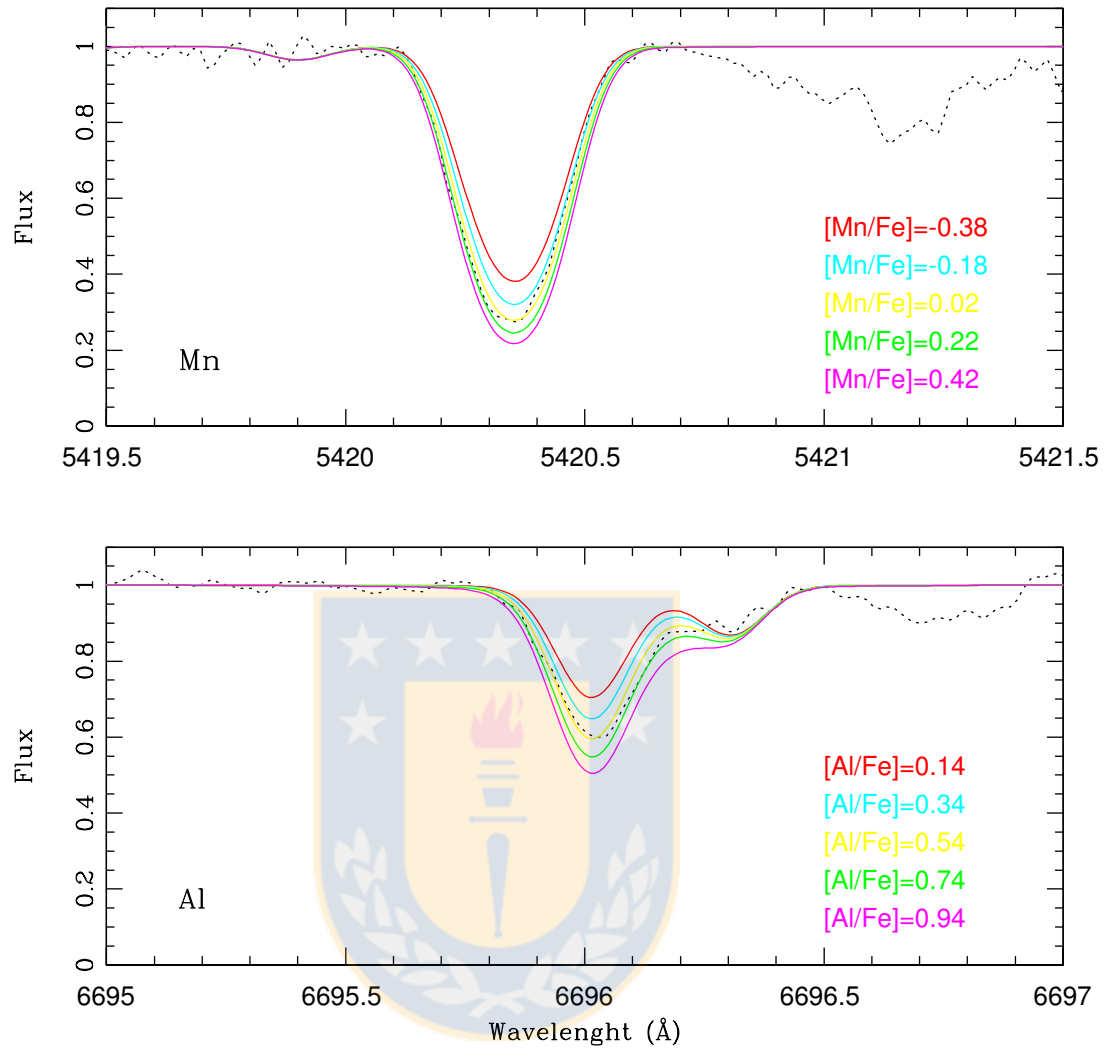
Figura 3.1: Manganese and Aluminum lines fitting process in Star #2. Dashed lines correspond to observed lines and continuous color lines are synthesised spectra for different abundances.

Tabla 3.2: Chemical abundances derived from our FLAMES/UVES data. First column: Elements ID. Columns 2-8: Abundances derived from our observed stars. Column 9: NGC-5927 mean abundance. Column 10: Solar abundances adopted for the analysis.

El	1	2	3	4	5	6	7	Cluster[1]	Sun
$[O/Fe]$	0.4	0.08	0.39	0.24	0.13	0.18	0.18	0.23$\pm$ 0.05	8.83
$[Na/Fe]_{NLTE}$	0.07	0.33	0.24	0.24	0.29	0.08	-0.02	0.18$\pm$ 0.05	6.32
$[Mg/Fe]$	0.30	0.30	0.22	0.25	0.29	0.22	0.30	0.27$\pm$ 0.02	7.55
$[Al/Fe]$	0.48	0.55	0.35	0.59	0.56	0.44	0.45	0.49$\pm$ 0.03	6.43
$[Si/Fe]$	0.24	0.13	0.29	0.12	0.31	0.24	0.32	0.24$\pm$ 0.03	7.61
$[Ca/Fe]^*$	0.19	0.15	0.08	0.15	0.15	0.17	0.13	0.15$\pm$ 0.01	6.39
$[Sc/Fe]$	0.35	0.32	0.23	0.34	0.32	0.41	0.29	0.32$\pm$ 0.02	3.12
$[Ti/Fe]$	0.36	0.3	0.26	0.33	0.31	0.41	0.24	0.32$\pm$ 0.02	4.94
$[V/Fe]^*$	0.45	0.37	0.23	0.41	0.36	0.45	0.3	0.37$\pm$ 0.03	4.00
$[Cr/Fe]^*$	0.06	-0.01	-0.02	0.08	0.05	0.04	0.01	0.03$\pm$ 0.02	5.63
$[Mn/Fe]$	-0.14	0.04	-0.04	-0.05	-0.11	-0.14	-0.22	-0.09$\pm$ 0.03	5.37
$[Fe/H]^*$	-0.54	-0.49	-0.44	-0.47	-0.51	-0.37	-0.49	-0.47$\pm$ 0.02	7.50
$[Co/Fe]^*$	0.35	0.36	0.3	0.42	0.39	0.49	0.33	0.38$\pm$ 0.03	4.93
$[Ni/Fe]^*$	0.12	0.18	0.13	0.14	0.18	0.25	0.22	0.17$\pm$ 0.02	6.26
$[Cu/Fe]$	0.3	0.32	0.08	0.44	0.33	0.43	0.31	0.32$\pm$ 0.05	4.19
$[Zn/Fe]$	-0.06	-0.03	0.01	-0.21	-0.14	0.11	0.03	-0.04$\pm$ 0.04	4.61
$[Y/Fe]$	-0.06	-0.09	-0.28	-0.16	-0.11	-0.03	-0.31	-0.15$\pm$ 0.04	2.25
$[Zr/Fe]$	0.14	-0.08	0.2	0.03	0.02	-0.06	-0.08	0.02$\pm$ 0.05	2.56
$[Ba/Fe]$	0	-0.06	-0.13	-0.17	-0.03	-0.09	-0.08	-0.08$\pm$ 0.02	2.34
$[Ce/Fe]$	-0.26	-0.27	-0.2	-0.11	-0.21	-0.28	-0.3	-0.23$\pm$ 0.03	1.53
$[Nd/Fe]$	0.36	0.16	0.16	0.21	0.16	0.13	0.16	0.19$\pm$ 0.03	1.59
$[Eu/Fe]$	0.55	0.29	0.56	9.99	9.99	0.36	0.38	0.43$\pm$ 0.04	0.52

[1]The errors are statistical errors obtained from the mean.

*Elements measured by EWs.

Tabla 3.3: Columns 2-5: Differences in abundance measurements due to the variations of each atmospheric parameter. Column 6: Estimated total error due to atmospheric errors. Column 7: Observed dispersion

ID	$\Delta T_{eff} = +65k$	$\Delta log(g) = +0.09$	$\Delta v_t = +0.08$	$\Delta [Fe/H] = +0.03$	S/N	σ_{tot}	σ_{obs}
$\Delta([O/Fe])$	0.01	0.03	0.00	0.03	0.02	0.05	0.12
$\Delta([Na/Fe])$	0.02	-0.05	-0.05	-0.02	0.02	0.08	0.13
$\Delta([Mg/Fe])$	0.03	0.00	-0.05	0.01	0.03	0.07	0.04
$\Delta([Al/Fe])$	0.01	-0.02	-0.03	-0.01	0.03	0.05	0.08
$\Delta([Si/Fe])$	-0.02	0.00	-0.03	0.03	0.02	0.05	0.08
$\Delta([Ca/Fe])$	0.08	-0.01	-0.02	0.01	0.06	0.10	0.03
$\Delta([Sc/Fe])$	0.01	0.01	0.01	0.01	0.02	0.03	0.06
$\Delta([Ti/Fe])$	0.10	0.00	-0.03	0.00	0.05	0.12	0.06
$\Delta([V/Fe])$	0.11	-0.01	-0.04	-0.01	0.04	0.12	0.08
$\Delta([Cr/Fe])$	0.06	0.00	-0.01	0.00	0.04	0.07	0.04
$\Delta([Mn/Fe])$	0.08	-0.02	-0.02	0.00	0.03	0.09	0.08
$\Delta([Fe/H])$	0.04	0.01	-0.03	0.02	0.02	0.06	0.05
$\Delta([Co/Fe])$	0.04	0.02	-0.03	0.02	0.08	0.10	0.06
$\Delta([Ni/Fe])$	0.03	0.02	-0.04	0.03	0.07	0.09	0.05
$\Delta([Cu/Fe])$	-0.02	-0.02	-0.02	-0.02	0.05	0.06	0.12
$\Delta([Zn/Fe])$	-0.01	0.03	-0.04	0.04	0.05	0.08	0.11
$\Delta([Y/Fe])$	-0.04	0.01	-0.05	0.02	0.05	0.08	0.11
$\Delta([Zr/Fe])$	0.03	-0.01	-0.09	0.02	0.02	0.10	0.11
$\Delta([Ba/Fe])$	0.05	0.00	-0.02	0.04	0.03	0.07	0.06
$\Delta([Ce/Fe])$	-0.02	0.01	0.01	0.03	0.05	0.06	0.07
$\Delta([Nd/Fe])$	0.02	0.00	-0.01	0.00	0.04	0.05	0.08
$\Delta([Eu/Fe])$	0.00	0.02	0.00	0.03	0.03	0.05	0.08

Chapter 4

Results

This is the first chemical abundance study of NGC 5927 using high resolution spectra that covers a wide sample of elements (see Table 3.2) which are involved in different nucleosynthetic processes. The main purpose is to study chemically the evolution of the cluster and investigate possible MPs.. For the discussion, field stars from the Bulge, Halo and Disk are compare with our results. We are looking for possible features that could suggest a link between the cluster with any of these structures. Also, we compare our sample set with Bulge GC that have similar metallicities in order to compare their chemical behaviour with NGC 5927.

In the following sections, we present chemical abundances for iron-peak elements, α elements, light elements and heavy elements.

4.0.1   Iron-peak elements

The mean iron abundance value that we found is:

$$[Fe/H] = -0.47 \pm 0.02$$

The spread of iron values are within the errors (see Table 3.3) indicating no intrinsic spread on iron abundances.

A slightly different iron content of [Fe/H]=-0.39 dex was found by P17 using UVES and GI-RAFFE data. This difference in iron estimation between us and P17 is probably due to (1) Different linelists used for the abundance analysis and (2) The lower resolution of GIRAFFE spectra.

We considered Sc, V, Cr, Mn, Co, Ni, Cu, and Zn as iron-peak elements and their values are listed in Table 3.2. The Figure 4.1 show each iron-peak element compared with field stars from the

Halo and Disk and in some cases with Bulge field stars and Bulge GCs. Some of these elements (Sc, V, Co, Ni, Cu) show an interesting behaviour which relate the cluster to the Bulge rather than the Disk. This opens the discussion about the origins of NGC 5927, which is linked kinematically to the Thick Disk but under the chemical perspective, shows similarities with the Bulge structure and follows the same behaviour as a Bulge GCs.

No large spreads are observe in the iron-peak elements excepting star #3 in Cu. This star is considerably under-abundant having a value of [Cu/Fe]=0.08 dex comparable to the sun, far away from the observe range trend in Cu seen in its companions.

Figura 4.1: Iron peak abundances for Sc, V, Cr and Mn for stars of NGC 5927 plotted in filled blue circles. Filled green triangles: Thick Disk stars (Reddy et al., 2006), light blue: bulge field stars (Johnson et al., 2014). Open triangles are bulge GCs, orange: NGC 6441 (Gratton et al., 2006, 2007) and magenta: NGC 6440 (Muñoz et al. submitted)
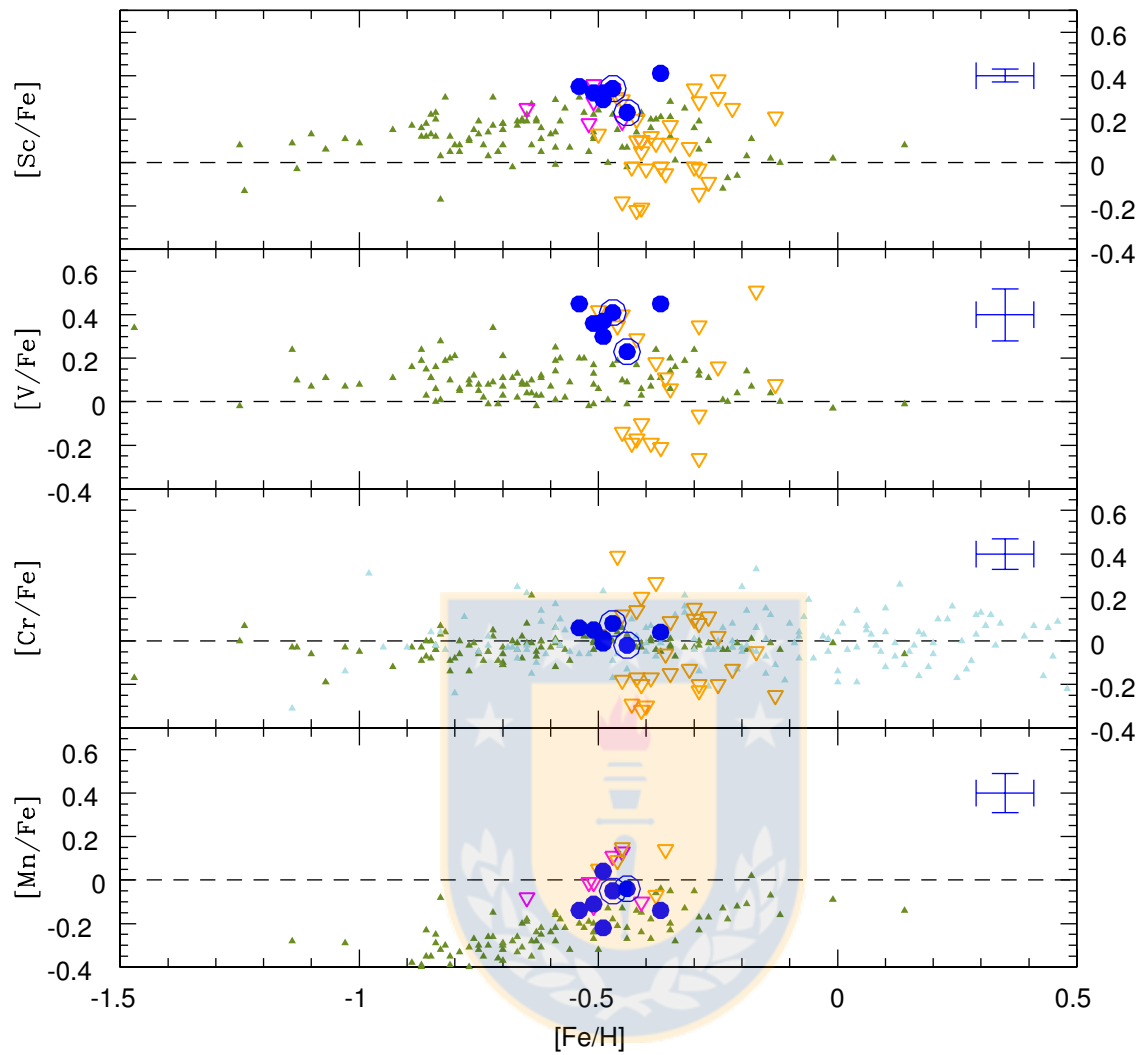
Figura 4.2: Iron peak abundances for Co, Ni, Cu and Zn for stars of NGC 5927 plotted in filled blue circles. Filled green triangles: Thick Disk stars (Reddy et al., 2006), light blue: bulge field stars (Johnson et al., 2014). Open triangles are bulge GCs, orange: NGC 6441 (Gratton et al., 2006, 2007) and magenta: NGC 6440 (Muñoz et al. submitted)
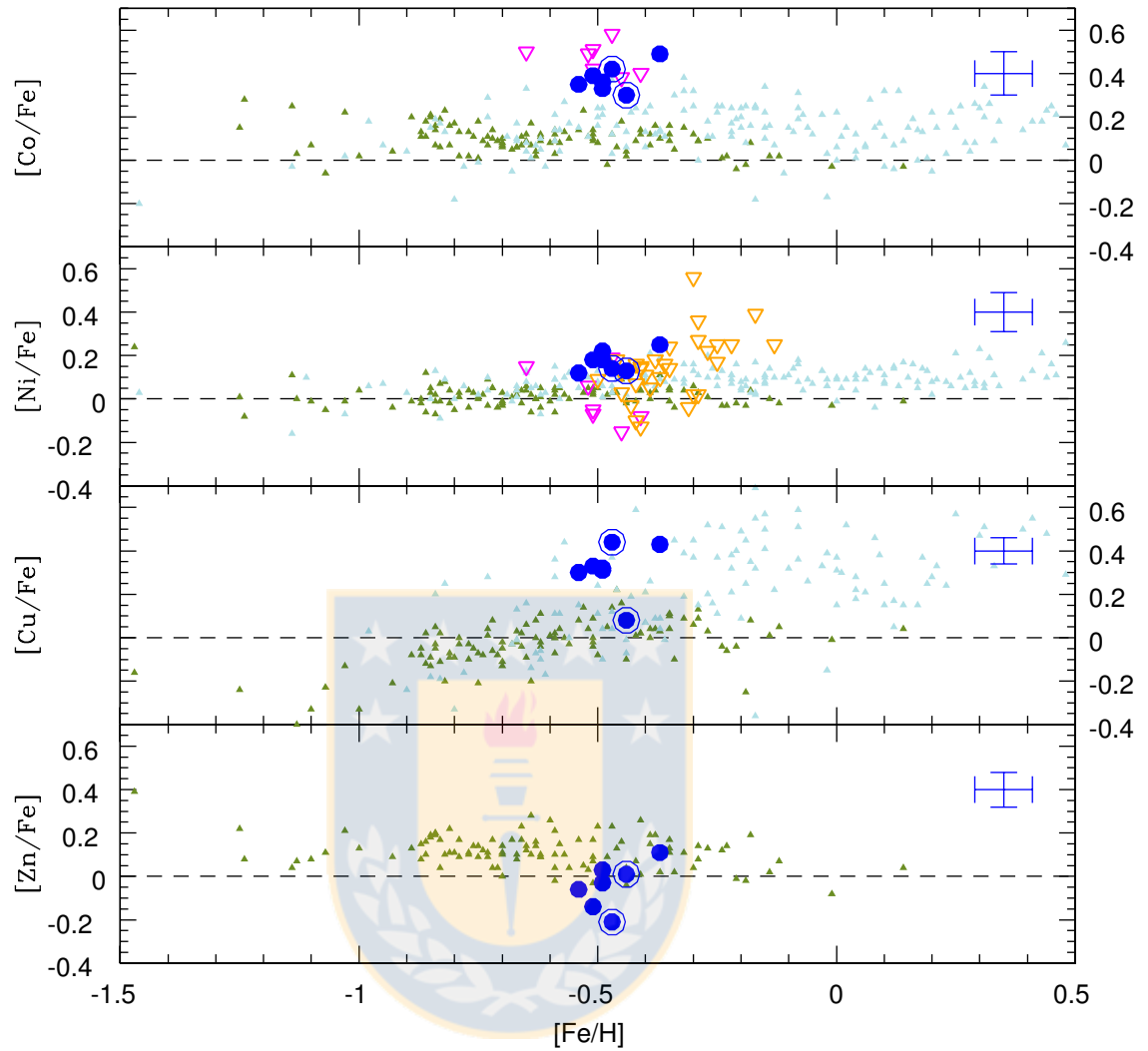
4.0.2 α elements

The α enhancement was obtained as the mean of Mg, Si, Ca and Ti. The O abundances are considered later as part of the Na-O anti-correlation. The mean value found for α elements is:

$$[\alpha/Fe] = 0.25 \pm 0.08$$

We also found a mean abundance for pure α elements of $[Ca + Si/Fe] = 0.19$ which is lower but consistent with the main value.

All the α elements in GGCs are over-abundant compared to the sun as can be seen in Figure 4.3 and NGC-5927 share this behaviour too as expected. This α element over-abundance is mainly the product of SNeII when massive stars exploded. Type II Supernovae are effective alpha-elements polluters who enrich the intra-cluster gas(Tinsley, 1979; Sneden, 2004).

The difference in α elements enhancement between the Thick Disk and Bulge are still under discussion and seems to be that both structures share the same α-enhancements. Bensby et al. (2010) compared type F and G dwarf field stars from the Disk and Bulge arguing that they are chemically similar. We did not include data from Bensby et al. (2010) for comparison due to the different type of star used for the study. Our comparison takes into account only giants because in our sample we have this kind of stars. In addition, Rojas-Arriagada et al. (2017, Figure 16) measured Mg for a considerable sample of star from the Disk and Bulge, finding no large difference between them.

In our field stars comparison sample, the α abundances in Bulge shows enhanced values with respect to Disk, but at metallicities of [Fe/H]$\sim$-0.7 they overlap as shown in Figure 4.4. The same behaviour is seen in each α element Mg, Si, Ca and Ti in Figure 4.3. We can observe in both Figures (4.4 and 4.3) that NGC 5927 is located just in the middle of the alpha trend of the Disk and Bulge. Also the cluster is compared with other Bulge GCs for each α element.

Besides the position in the Milky Way shown in Figure 2.2, NGC 5927 has kinematics consistent with being a member of the Thick Disk of the Galaxy (Allen et al., 2008; Casetti-Dinescu et al., 2007) suggesting it as one of the best Thick disk candidate GCs. From the chemical point of view, NGC 5927 has α-abundances that stand between Bulge and Disk values.
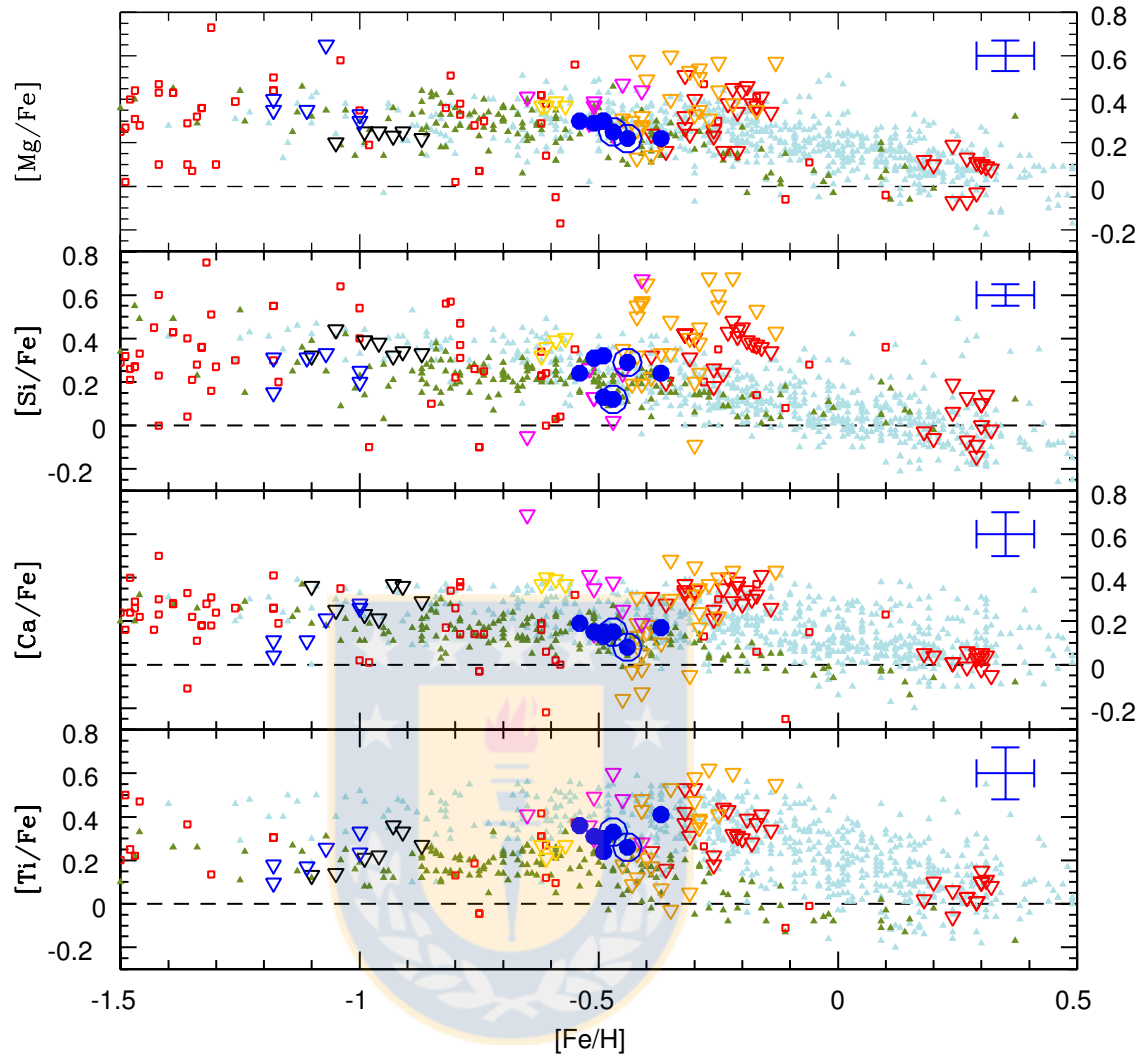
Figura 4.3: [Mg/Fe], [Si/Fe], [Ca/Fe] and [Ti/Fe] abundances versus [Fe/H] content in NGC-5927, are plotted in filled blue circles. Filled triangles are different scenarios. Green: Thick Disk stars (Reddy et al., 2006), Red: GGCs (Carretta et al., 2009b) except in Ti and Soft Pink: Bulge stars from Gonzalez et al. (2011). Open triangles represent different Bulge GCs, black: NGC-6723 (Rojas-Arriagada et al., 2016), blue: HP1 (Barbuy et al., 2016), yellow: NGC-6342 (Origlia et al., 2005), orange: (Gratton et al., 2006) and red: Terzan 5 (Origlia et al., 2011)
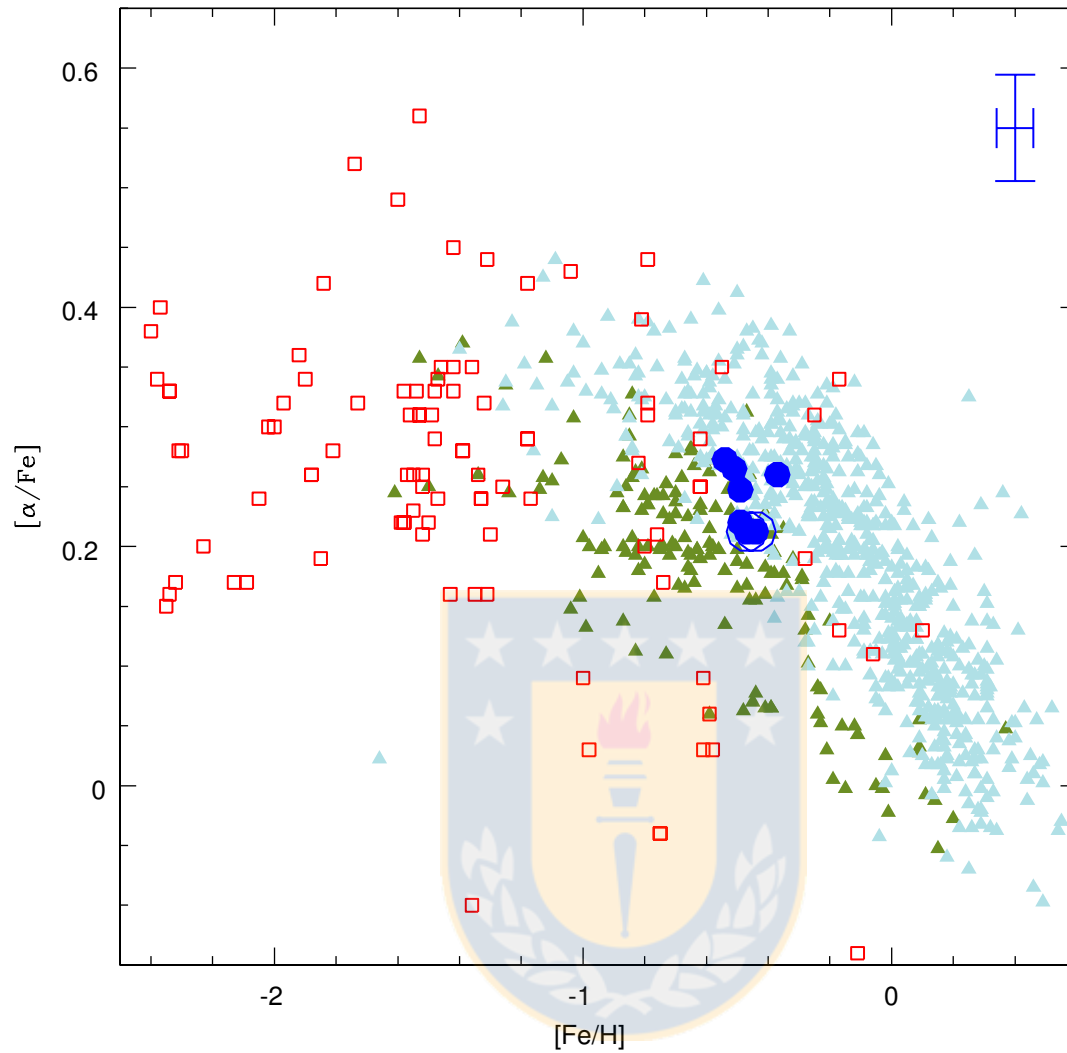
Figura 4.4: NGC-5927 is represented in filled blue circles. Filled triangles are different scenarios. Green: Thick Disk stars (Reddy et al., 2006), Red: GGCs (Carretta et al., 2009b) and Soft Pink: Bulge stars from Gonzalez et al. (2011). Open triangles represent different Bulge GCs, dark blue: NGC-6723 (Rojas-Arriagada et al., 2016), yellow: NGC-6342 (Origlia et al., 2005), orange: (Gratton et al., 2006) and red: Terzan 5 (Origlia et al., 2011)

4.0.3 Light elements

In GCs, light elements shows variations in their abundances. The responsible processes for these variations are different proton capture chains in star of previous generations. In the CNO cycle, N is enhanced while C and O are depleted, also in the Ne-Na cycle Ne is depleted and Na enhanced and for the Mg-Al cycle Mg is depleted and Al enhanced. The observation of these abundance differences tell us about the MPs phenomenon. In NGC 5927 we observe a spread in O, Na and Al larger than internal errors indicating a real spread in these elements, and thus confirming that this cluster contains MPs. However, the observed dispersion in Mg is within the range expected from errors alone, suggesting no intrinsic variation (See Table 3.3). In the following, we discuss about the relations between these elements, looking for features in NGC 5927 in order to understand its MPs.

4.0.3.1 Na-O anticorrelation

In almost every GC an anti-correlation exist between O and Na and it has been well studied in many of them (e.g. Carretta et al. (2009b)). This anti-correlation is one of the most important chemical signature of MPs since we can differentiate populations along the extension of the anti-correlation (Carretta et al. (2009a)). In the case of NGC 5927, the first study of the O-Na anti-correlation was performed by P17 and their results are in good agreement with us. The main difference in the Na values in P17 with respect to our measurements are due to the fact that we take NLTE correction on Na into account. The offset in Sodium between the two datasets is ~ 0.2 dex.

The Figure 4.6 shows Na as a function of O and the Na abundances distribution. In our sample, Na seems to be distributed in two groups suggesting a possible bi-modality distribution. Of course, our small sample may not be statistical significant and more data are required to verify this behaviour. The mean [Na/Fe] in Na-rich (#2, #3, #4, #5) and Na-poor (#1, #6, #7) groups is 0.28 dex and 0.04 dex respectively, both with a standard deviation of 0.04. However this bi-modality can be observed in P17 (Figure 2) as well.

We also compared our results with GCs stars from Carretta et al. (2009a) and Bulge GCs with similar metalicities as shown in Figure 4.5. We confirm the existence of the O-Na anti-correlation exists, but it is not very extended.
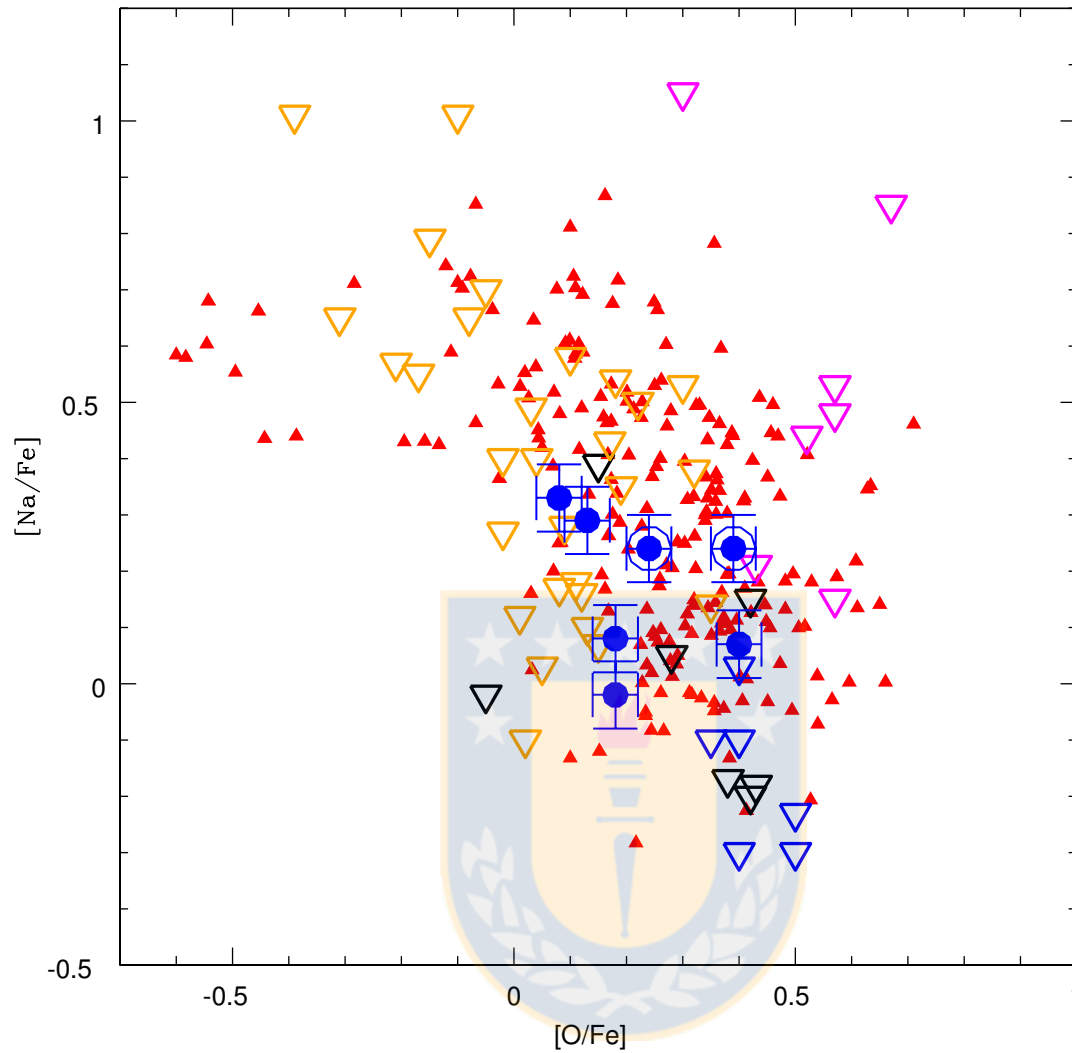
Figura 4.5: O-Na anti-correlation for NGC-5927 in filled blue squares and filled red triangles represent 214 red giants from 19 clusters with UVES (Carretta et al., 2009b). Open triangles represent different Bulge GCs. Black: NGC 6723 (Rojas-Arriagada et al., 2016), blue: HP1 (Barbuy et al., 2016), orange: NGC 6441 (Gratton et al., 2006, 2007) and magenta NGC 6440 (Muñoz et al. submitted)

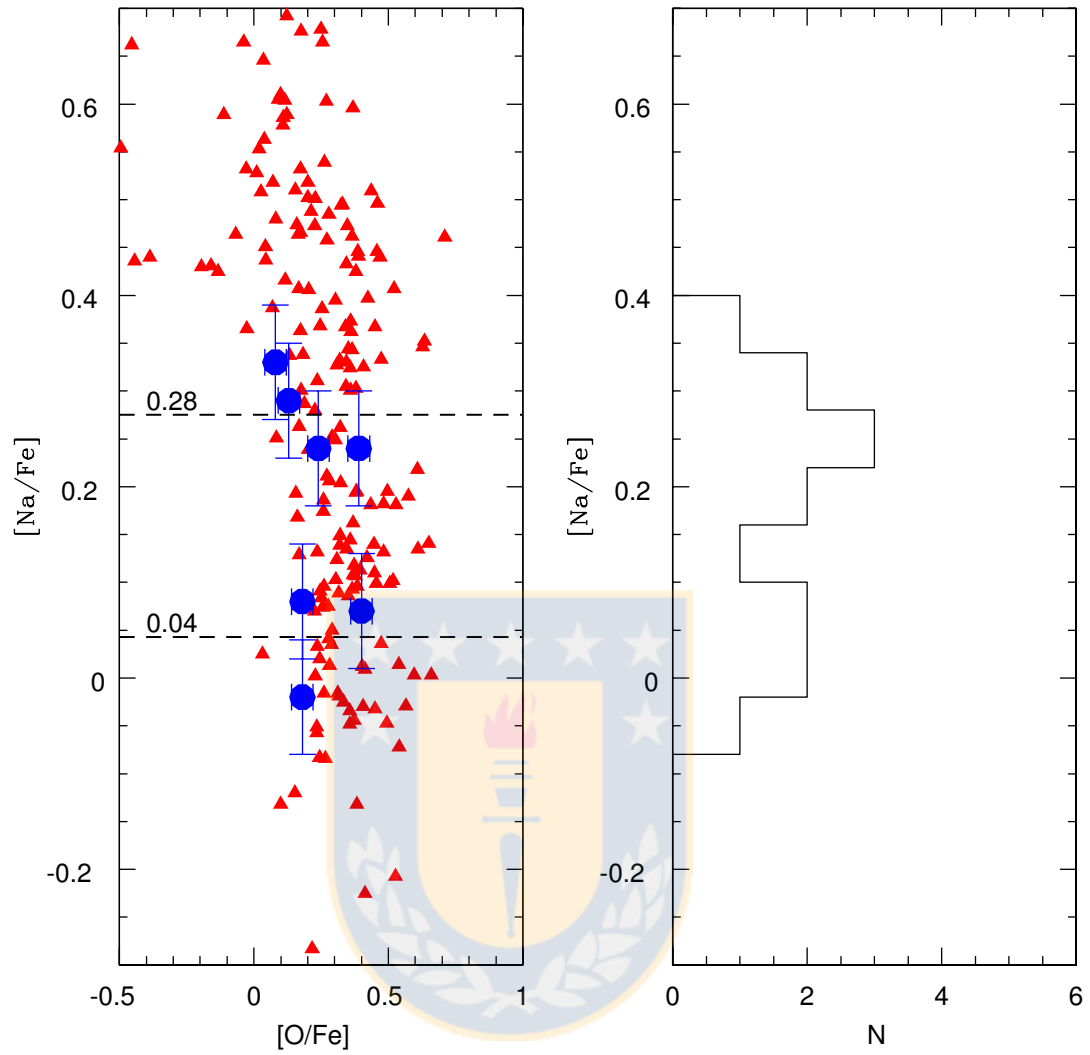Figura 4.6: Left: O-Na anticorrelation. Filled blue squares for NGC-5927 and filled red triangles represent 214 red giants from the 19 clusters with UVES (Carretta et al., 2009b). Right: [Na/Fe] shows a bimodal distribution. The SG observed in the diagram correspond to the $\sim 70\%$ which is in good agreement with the generation percentage acording to Carretta et al. (2009b).

4.0.3.2   Mg-Al anticorrelation

Unlike Na-O, the Mg-Al anti-correlation is only present in some GCs (Carretta et al., 2009a). In the case of NGC 5927, no signs of a clear anti-correlation can be distinguish in Figure 4.7 where our Mg values shows an under abundance compared with the trend of Carretta et al. (2009b) stars sample. This offset in Mg is possibly due to the fact that the metallicity of NGC 5927 ([Fe/H]=-0.47 dex) is out of the range of metallicity considered on Carretta et al. (2009a) sample. Nontheless, this behaviour is shared with other two Bulge GCs with similar metallicity. The values in Al instead, are over-abundant compared with field stars from Halo and Disk and enhanced by ~ 0.2 dex compared to Mg.

The Mg-Al analysis in NGC 5927 performed by P17 (Figure 3) include data from UVES and GIRRAFE. They also observe no signs of anti-correlation and the abundances in Mg and Al are in good agreement with us.

4.0.3.3   Na-Al correlation

The correlation between Na and Al in GCs it is probably due to the Ne-Na and Mg-Al chain activation in previous generations where massive stars enhanced Na and Al respectively. For the case of NGC 5927 we observe a correlation between Na and Al in Figure 4.8 even when we do not see a clear anti-correlation in Mg-Al (See Section 4.0.3.2). The correlation is not continuous due to the Na distribution, grouping it in two groups as is described in Section 4.0.3.1. The presence of a Na-Al correlation without a Mg-Al anti-correlation has been observed before in other GCs (e.g. M4 by Marino et al. (2008)). We attribute this behaviour in NGC 5927 to a possible activation of the Mg-Al chain reaction in previous generation but with a slow rate.

The linear fit used for the correlation has an slope of $a = +0.39$ with an error of ± 0.11. This fit was made excluding Star #3 which is the most Al-poor one and shows chemical behaviours (mostly under-abundances) that do not follow the trends described by their companions. The significance of the slope is about 3.5σ. The anomalies in star #3 as can be seen also in Figure 4.7 for Mg-Al and Figure 4.1 for iron-peak elements (specially in Cu).
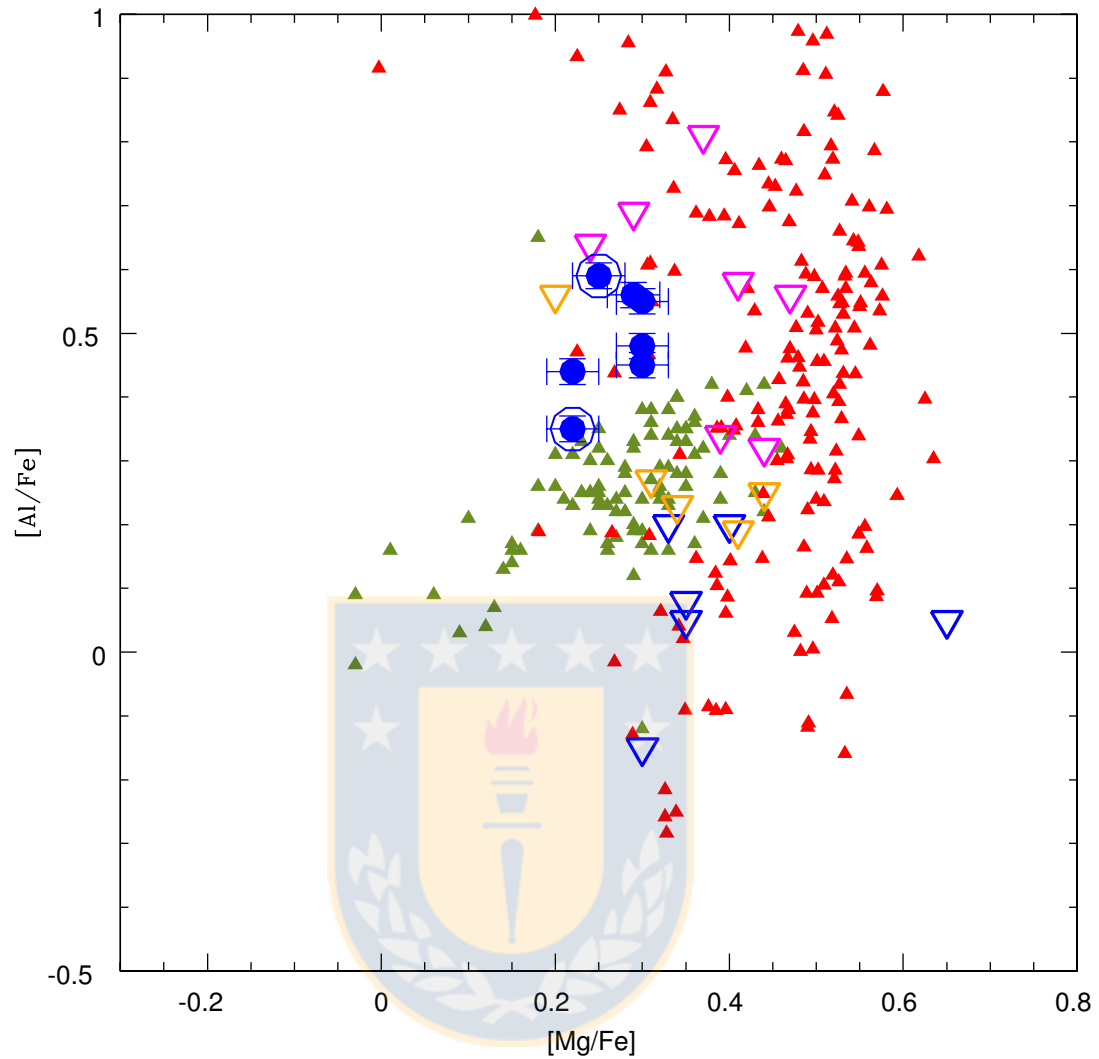
Figura 4.7: Mg-Al on NGC-5927 in filled blue circles, filled red triangles represent 214 red giants from 19 clusters with UVES (Carretta et al., 2009b) and filled green triangles are field stars from Thick Disk stars (Reddy et al., 2006). Open triangles are stars from different GCs. Black: NGC 6723 (Rojas-Arriagada et al., 2016), blue: HP1 (Barbuy et al., 2016), orange: NGC 6440 (Gratton et al., 2006, 2007) and magenta NGC 6440 (Muñoz et al. submitted)

Figura 4.8: Na-Al correlation for NGC 5927 in filled blue squares and filled red triangles represent 214 red giants from 19 clusters with UVES (Carretta et al., 2009b). Open triangles represent different Bulge GCs. Black: NGC 6723 (Rojas-Arriagada et al., 2016), blue: HP1 (Barbuy et al., 2016), orange: NGC 6441 (Gratton et al., 2006, 2007) and magenta NGC 6440 (Muñoz et al. submitted). Dashed is the best fit for NGC 5927 excluding Star #3.
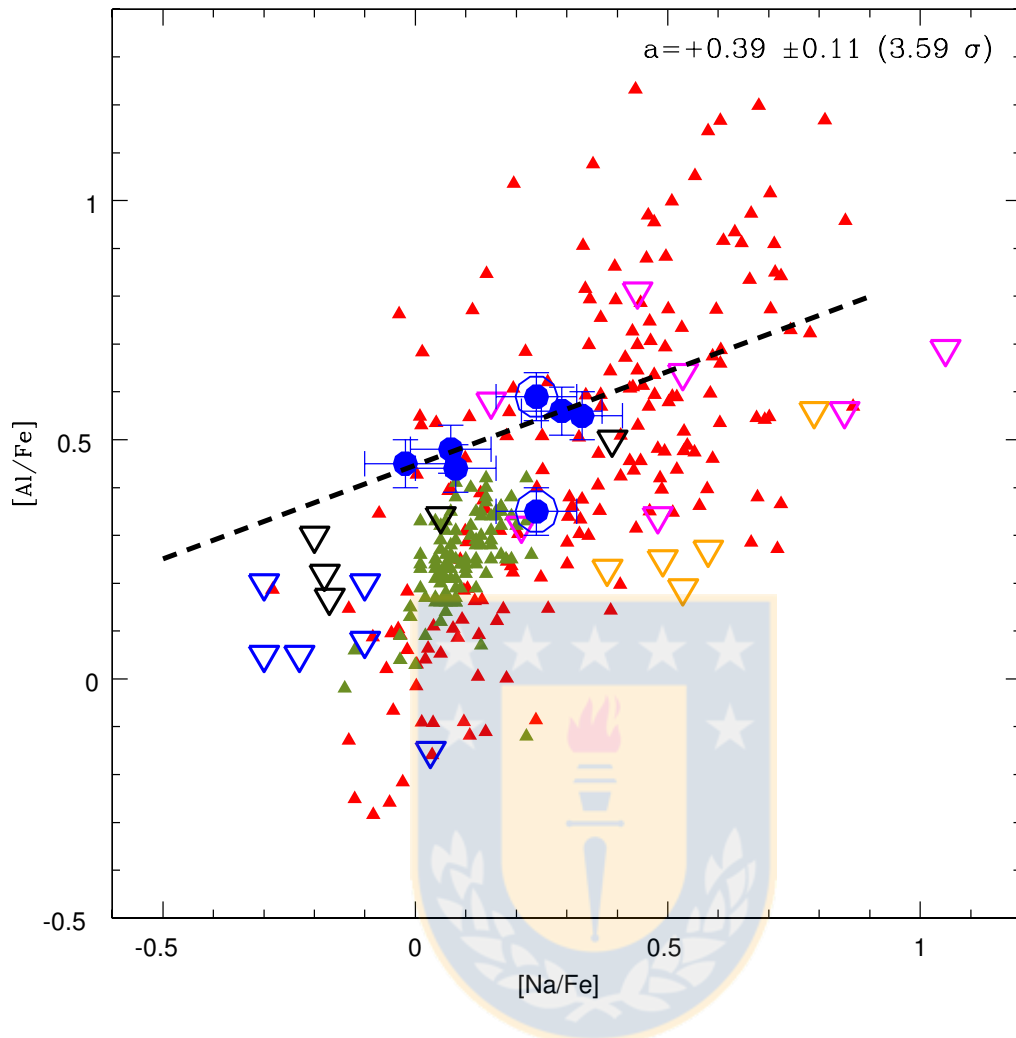
4.0.4   Heavy elements

The neutron capture is the nuclear reaction process responsible for the formation of heavy elements. Depending on the neutron capture rate, we can separate these process in two types: (1) When the capture time is longer than the beta-decay, it is called s-process. (2) If the neutron capture is faster than the beta-decay, we have the r-process.

The elements mainly produced by s-process can be light-s elements such as Y, Zr and heavy-s elements like Ba and Ce. This process occurs principally in the AGB phase of intermediate mass stars. On the other hand, the r-process elements are mainly generated during the SNe II explosions. One of the elements produced mainly by this process is Eu which can be used to determine how strong is the contribution of the process in the chemical evolution of the cluster. Also, SNeII produces iron-peak elements and α-elements.

In Figure 4.10 we compare Y, Ba and Eu abundances of NGC 5927 with field stars and also with Bulge GCs. For Y and Ba, abundance values are sub-solar and shows some differences with respect to the Bulge GCs, with the exception of NGC 6440. We underline the strong similarities in heavy elements enhancements between NGC 5927 and NGC 6440. These similarities have also been observed in the α and iron-peak elements (Sections 4.0.2 and 4.0.1 respectively). For Eu instead, values are over-abundant with respect to the Sun. This indicates a large contribution of SNeII to the proto-cluster cloud.

Since Ba is mainly processed by s-process and Eu mainly by r-process, the [Ba/Eu] ratio is an indicator of which process contributed more in the chemical evolution of the cluster. In Figure 4.9, we observe that [Ba/Eu] ratio in NGC 5927 is mainly dominated by r-process contributions. This suggest that the early proto-cluster environment was polluted mainly by SNeII. In addition, is notable the similarity (again) between NGC 5927 and NGC 6440 showing values very similar indicating that both cluster share similar evolutionary scenarios.
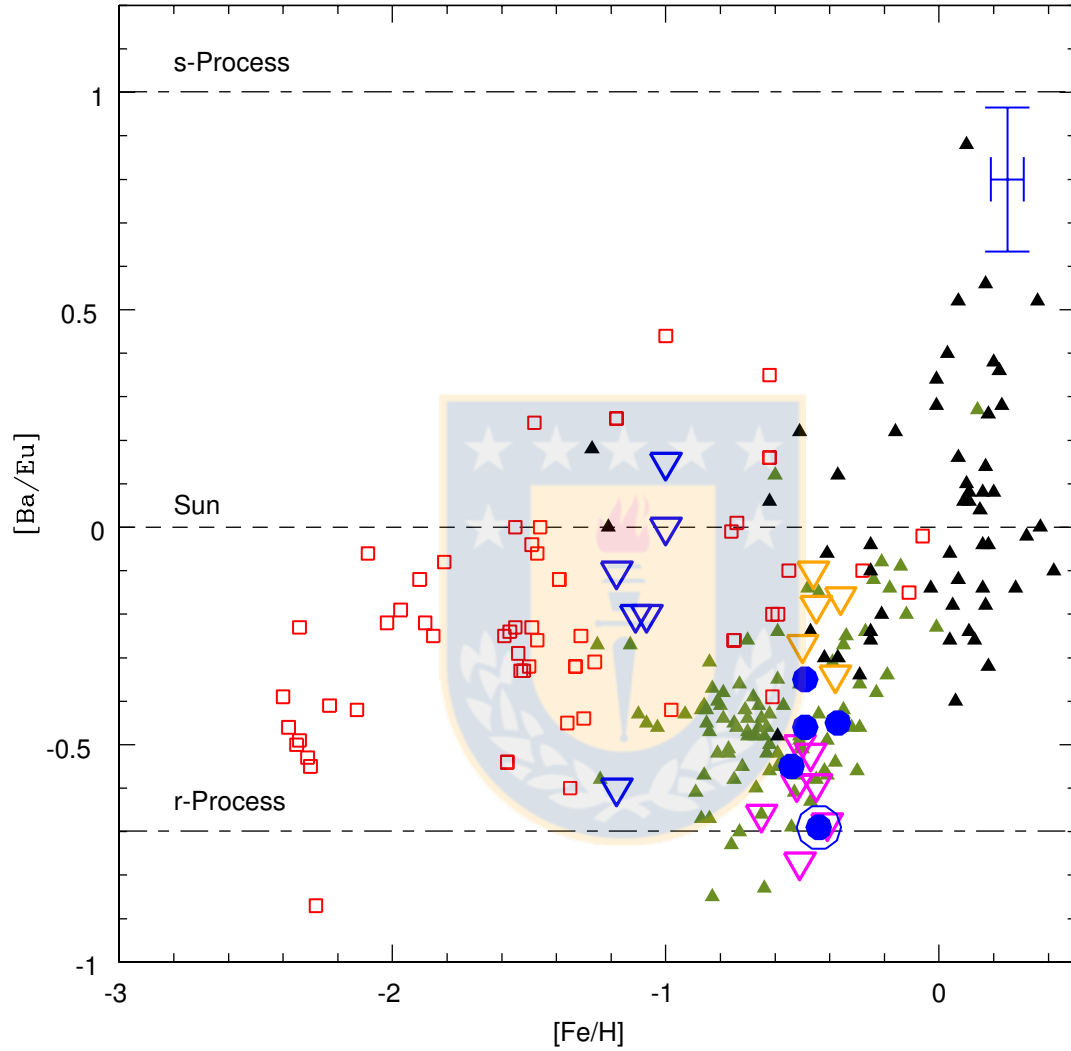
Figura 4.9: [Be/Eu] ratio as function of [Fe/H]. In filled blue circles, NGC 5927. Filled triangles are different scenarios. Green: Thick Disk stars (Reddy et al., 2006) and black: Bulge field stars (Van der Swaelmen et al., 2016). Open red squares: GGCs (Pritzl et al., 2005). Open triangles represent different Bulge GCs, orange: NGC 6441 (Gratton et al., 2006), blue HP1 (Barbuy et al., 2016) and magenta NGC 6440 (Muñoz et al. submitted)
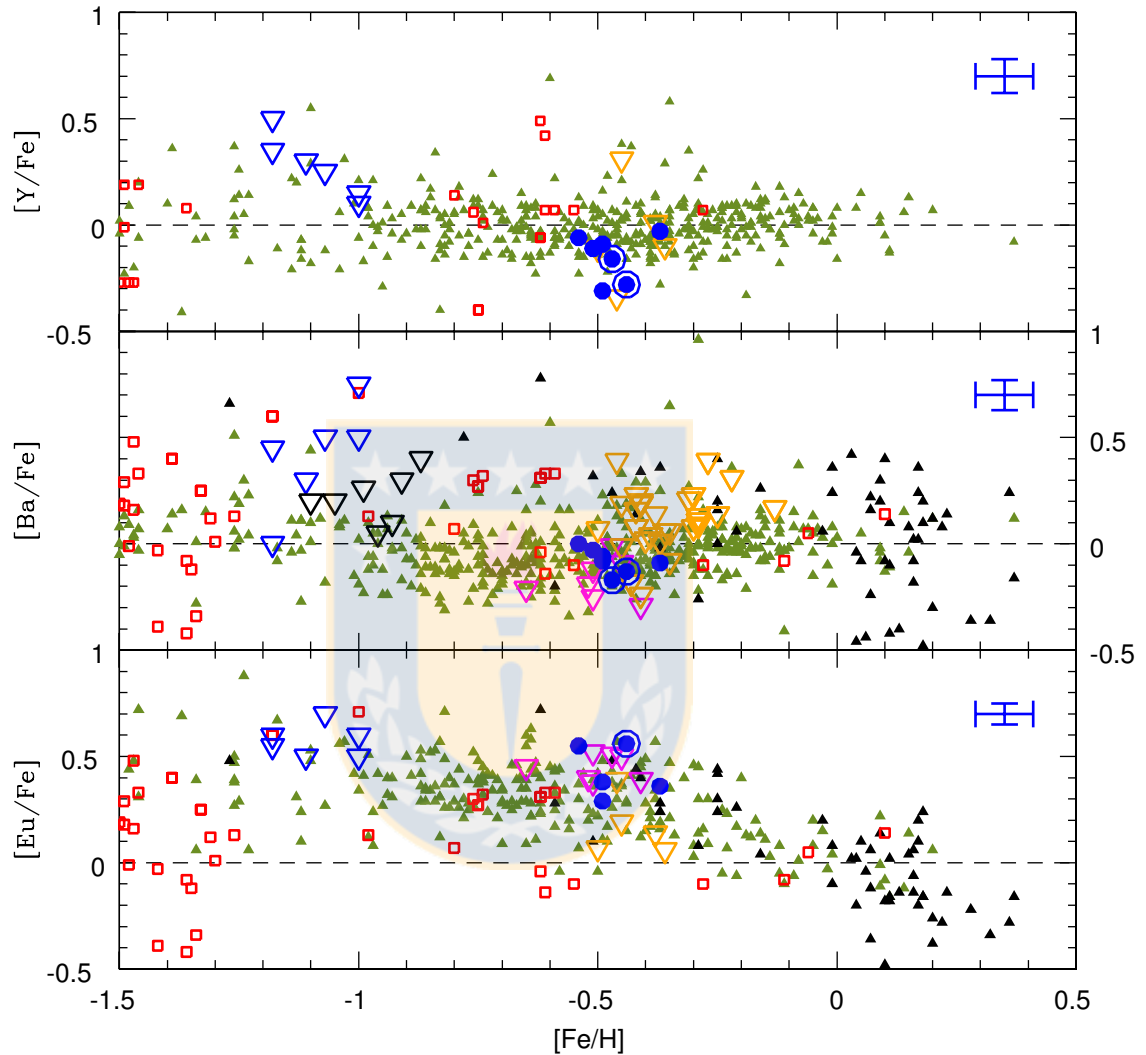
Figura 4.10: Heavy elements values as function of [Fe/H]. NGC 5927 is represented in filled blue circles. Filled triangles are different scenarios. Green: Thick Disk stars (Reddy et al., 2006), black: Bulge field stars (Van der Swaelmen et al., 2016). Open red squares are GCs stars Pritzl et al. (2005) Open triangles represent different Bulge GCs, black: NGC 6723 (Rojas-Arriagada et al., 2016), blue: HP1 Barbuy et al. (2016), orange: NGC 6440 (Gratton et al., 2006) and magenta NGC 6440 (Muñoz et al. submitted)

Chapter 5

Sumary and Conclusions

In this paper we present a detailed chemical abundances analysis of the Globular Cluster NGC 5927. A total of 22 elements in 7 giant stars are consider for the analysis using high resolution spectroscopy taken by UVES instrument with a moderate S/N ($\sim$ 40). We measure 16 elements by spectrum-synthesis and 7 elements by EW, including an accurate error analysis. The results are compared with different components of the Milky Way such as Halo, Disk and Bulge field stars and Bulge GCs. We obtained the following results:

- We found a mean metallicity of [Fe/H]=-0.47 dex with a $\sigma_{obs} = 0.02$. This value is in good agreement with the value estimated by Harris (1996, 2010 ed.) ([Fe/H]=-0.49). Also we rule out an intrinsic spread in the iron content. No significant spread is visible in other iron-peak elements. For some elements, NGC 5927 seem to follow the Bulge trend rather than the Disk. Previous literature refers to NGC 5927 as one of the most metal-rich Thick Disk GCs but its metallicity is comparable with the Bulge field stars and Bulge GCs (ie. NGC 6440). There is a difference of $\sim$ 0.1 dex between our measurements and Pancino & the GES collaboration (2017) ([Fe/H]=-0.39 dex).

- We confirm the existence of an anti-correlation between O and Na but the spread in O is small. The Na distribution seem to be bi-modal but we caution that our sample size is small. A large sample is required to confirm this behaviour.

- We observe no clear evidence for Mg-Al anti-correlation in NGC 5927, however we observe a Na-Al correlation. The spread in Al may indicate a low Mg-Al cycle activity. Also, our abundances are in good agreement with Pancino & the GES collaboration (2017) in this topic.

- About α content, NGC 5927 matches the typical trends of the Galaxy field stars. We found an alpha enrichment of [α/Fe]=0.25 ±0.08. In each α element (Mg, Si,Ca and Ti), the values for NGC 5927 are not so enhanced as those for Bulge GCs but they still are over-abundant. These enhancements indicate that the cluster has experienced rapid chemical evolution which is related to contributions from SNeII. We decide not to relate NGC 5927 with the Bulge or Disk components using alpha abundances, since whether there exists a difference in alpha abundance between these two components is still under debate.

- A strong contribution of r-process is suggested by analysing [Ba/Eu] ratios pointing out SNeII as principal polluter for the proto-cluster cloud.

- The heavy s-process elements shows no significant spread, which seems to contradict the theory that AGB stars are polluters for the second generation stars.

- We highlight the similarity of NGC 5927 with NGC 6440 Bulge GC in α, iron-peak and heavy elements, suggesting similar origins between these two GCs.

- Star #3 shows anomalies abundances with respect to the other stars of the sample. We attribute this behaviour to some problem with the spectrum of star #3. Also exist a very low probability, but still possible, that this star may be a field star, even when it passed all the membership criteria.

- This is the first chemical study that involves a wide range of elements measured with good accuracy, but due to the small size of the sample, our findings cannot be conclusive. More data is required in order to have a better understanding the chemical evolution of this very interesting cluster.

In addition, considering that NGC 5927 (1) is a very old GC with an age between 10.7 Gyr VandenBerg et al. (2013) and 12.25 Gyr (Dotter et al., 2010), as old as the Milky Way itself; (2) its calculated orbit using proper motions (Allen et al., 2008) take place between 4 and 6 kpc; (3) the iron-peak enhancement in some elements follows the Bulge trend rather than the Disk and; (4) the chemical similarities with Bulge GCs and specially with NGC 6440, lead us to consider a formation scenario where the cluster was formed from material between the Bulge and Disk, both still in formation. The gas in this region of transition left chemical traces in NGC 5927 with its properties inbetween the Bulge and the Disk observed today.

Bibliography

Adibekyan V. Z., Sousa S. G., Santos N. C., Delgado Mena E., González Hernández J. I., Israelian G., Mayor M., Khachatryan G., 2012, aap, 545, A32

Allen C., Moreno E., Pichardo B., 2008, apj, 674, 237

Armandroff T. E., Zinn R., 1988, aj, 96, 92

Barbuy B., et al., 2016, aap, 591, A53

Beaulieu S. F., Freeman K. C., Kalnajs A. J., Saha P., Zhao H., 2000, aj, 120, 855

Bensby T., Feltzing S., Lundström I., 2003, aap, 410, 527

Bensby T., et al., 2010, aap, 512, A41

Bland-Hawthorn J., Gerhard O., 2016, araa, 54, 529

Caloi V., D'Antona F., 2011, mnras, 417, 228

Carretta E., et al., 2009a, aap, 505, 117

Carretta E., Bragaglia A., Gratton R., Lucatello S., 2009b, aap, 505, 139

Carretta E., Bragaglia A., Gratton R., D'Orazi V., Lucatello S., 2009c, aap, 508, 695

Casetti-Dinescu D. I., Girard T. M., Herrera D., van Altena W. F., López C. E., Castillo D. J., 2007, aj, 134, 195

Cayrel R., et al., 2004, aap, 416, 1117

D'Antona F., Caloi V., Montalbán J., Ventura P., Gratton R., 2002, aap, 395, 69

Decressin T., Meynet G., Charbonnel C., Prantzos N., Ekström S., 2007, aap, 464, 1029

Dekker H., D'Odorico S., Kaufer A., Delabre B., Kotzlowski H., 2000, in Iye M., Moorwood A. F., eds, procspie Vol. 4008, Optical and IR Telescope Instrumentation and Detectors. pp 534–545, doi:10.1117/12.395512

Denisenkov P. A., Denisenkova S. N., 1989, Astronomicheskij Tsirkulyar, 1538, 11

Dotter A., et al., 2010, apj, 708, 698

Francois P., 1991, aap, 247, 56

Fulbright J. P., 2000, aj, 120, 1841

Gilmore G., Reid N., 1983, mnras, 202, 1025

Gonzalez O. A., et al., 2011, aap, 530, A54

Gratton R. G., Carretta E., Matteucci F., Sneden C., 2000, aap, 358, 671

Gratton R. G., Lucatello S., Bragaglia A., Carretta E., Momany Y., Pancino E., Valenti E., 2006, aap, 455, 271

Gratton R. G., et al., 2007, aap, 464, 953

Harris W. E., 1996, aj, 112, 1487

Heitsch F., Richtler T., 1999, aap, 347, 455

Johnson C. I., Rich R. M., Kobayashi C., Kunder A., Koch A., 2014, aj, 148, 67

Kurucz R. L., 1970, SAO Special Report, 309

Langer G. E., Hoffman R., Sneden C., 1993, pasp, 105, 301

Marino A. F., Villanova S., Piotto G., Milone A. P., Momany Y., Bedin L. R., Medling A. M., 2008, aap, 490, 625

Mashonkina L., Gehren T., 2001, aap, 376, 232

Minniti D., 1996, apj, 459, 579

Murdin P., 2001, Encyclopedia of Astronomy & Astrophysics. Taylor & Francis, https://books.google.cl/books?id=W8zLQgAACAAJ

Oort J. H., 1977, araa, 15, 295

Origlia L., Valenti E., Rich R. M., 2005, mnras, 356, 1276

Origlia L., et al., 2011, apjl, 726, L20

Ortolani S., Renzini A., Gilmozzi R., Marconi G., Barbuy B., Bica E., Rich R. M., 1995, nat, 377, 701

Pagel B., 1997, Nucleosynthesis and Chemical Evolution of Galaxies. Cambridge University Press, https://books.google.cl/books?id=Gd_L9binuDsC

Pancino E., the GES collaboration 2017, preprint, (arXiv:1702.06083)

Pritzl B. J., Venn K. A., Irwin M., 2005, aj, 130, 2140

Reddy B. E., Tomkin J., Lambert D. L., Allende Prieto C., 2003, mnras, 340, 304

Reddy B. E., Lambert D. L., Allende Prieto C., 2006, mnras, 367, 1329

Renzini A., Buzzoni A., 1986, in Chiosi C., Renzini A., eds, Astrophysics and Space Science Library Vol. 122, Spectral Evolution of Galaxies. pp 195–231, doi:10.1007/978-94-009-4598-2˙19

Rich R. M., Reitzel D. B., Howard C. D., Zhao H., 2007, apjl, 658, L29

Rojas-Arriagada A., Zoccali M., Vásquez S., Ripepi V., Musella I., Marconi M., Grado A., Limatola L., 2016, aap, 587, A95

Rojas-Arriagada A., et al., 2017, preprint, (arXiv:1704.03325)

Rutledge G. A., Hesser J. E., Stetson P. B., 1997, pasp, 109, 907

Schuster W. J., Moitinho A., Márquez A., Parrao L., Covarrubias E., 2006, aap, 445, 939

Simmerer J., Feltzing S., Primas F., 2013, aap, 556, A58

Sneden C., 1973, apj, 184, 839

Sneden C., 2004, memsai, 75, 267

Sofue Y., Honma M., Omodaka T., 2009, pasj, 61, 227

Tinsley B. M., 1979, apj, 229, 1046

Van der Swaelmen M., Barbuy B., Hill V., Zoccali M., Minniti D., Ortolani S., Gómez A., 2016, aap, 586, A1

VandenBerg D. A., Brogaard K., Leaman R., Casagrande L., 2013, apj, 775, 134

Villanova S., Geisler D., 2011, aap, 535, A31

Villanova S., Geisler D., Carraro G., Moni Bidin C., Muñoz C., 2013, apj, 778, 186

Zoccali M., et al., 2003, aap, 399, 931

de Mink S. E., Pols O. R., Langer N., Izzard R. G., 2009, Proceedings of the International Astronomical Union, 5, 169